



HAL
open science

Understanding the langmuir and Langmuir-Schaefer film conformation of low-bandgap polymers and their bulk heterojunctions with PCBM

Edilene Silva, Alberto Gregori, José Fernandes, Christian Njel, Rémi Dedryvère, Carlos Constantino, Roger C. Hiorns, Christine Lartigau-Dagron, Clarissa Olivati

► To cite this version:

Edilene Silva, Alberto Gregori, José Fernandes, Christian Njel, Rémi Dedryvère, et al.. Understanding the langmuir and Langmuir-Schaefer film conformation of low-bandgap polymers and their bulk heterojunctions with PCBM. *Nanotechnology*, 2020, 31 (31), pp.315712. 10.1088/1361-6528/ab8b0b . hal-02860465

HAL Id: hal-02860465

<https://hal.science/hal-02860465>

Submitted on 12 Sep 2023

HAL is a multi-disciplinary open access archive for the deposit and dissemination of scientific research documents, whether they are published or not. The documents may come from teaching and research institutions in France or abroad, or from public or private research centers.

L'archive ouverte pluridisciplinaire **HAL**, est destinée au dépôt et à la diffusion de documents scientifiques de niveau recherche, publiés ou non, émanant des établissements d'enseignement et de recherche français ou étrangers, des laboratoires publics ou privés.

1
2
3 **Understanding the Langmuir and Langmuir-Schaefer film Conformation of**
4
5
6 **low-Bandgap Polymers and their Bulk Heterojunctions with PCBM**
7
8
9

10 *Edilene A. Silva^{a,b}, Alberto Gregori^{b,c}, José D. Fernandes^a, Christian Njel^d, Remi Dedryvère^b,*
11
12 *Carlos J. L. Constantino^a, Roger C. Hiorns^b, Christine Lartigau-Dagron^{b*}, Clarissa A. Olivati^{b*}*
13
14

15 ^a Departamento de Física, Faculdade de Ciências e Tecnologia, UNESP, Rua Roberto Simonsen
16
17 305, Presidente Prudente, SP, Brazil.
18
19

20 ^b Université de Pau et des Pays de l'Adour, E2S UPPA, CNRS, IPREM, Pau, France
21

22 ^c Center for Sustainable Future Technologies, Istituto Italiano di Tecnologia, via Livorno 60,
23
24 10144 Turin, Italy
25

26 ^d Karlsruhe Institute of Technology (KIT), Hermann-von-Helmholtz-Platz 1, Eggenstein-
27
28 Leopoldshafen, 76344, Germany
29
30

31
32
33
34
35
36 **Corresponding authors:** christine.lartigau-dagron@univ-pau.fr and olivati@fct.unesp.br.
37

38
39 **Authors e-mails:** eassuncaosilva@gmail.com, gregori.alberto@gmail.com,
40
41 fernandes.j.diego@gmail.com, christian.njel@hotmail.fr, remi.dedryvere@univ-pau.fr,
42
43 carlos.constantino@unesp.br, roger.hiorns@univ-pau.fr.
44
45
46
47
48

49 **KEYWORDS:** low-bandgap polymers, Langmuir-Schaefer, monolayers, bulk heterojunction,
50
51 structure-property relations.
52
53
54
55
56
57
58
59
60

ABSTRACT

Low-bandgap polymers are widely used as a p-type components in photoactive layers of organic solar cells, due to their ability to capture a large portion of the solar spectrum. The comprehension of their supramolecular assembly is crucial in achieving high-performance organic electronic devices. Here we synthesized two exemplar low-bandgap cyclopentadithiophene (CPDT):diketopyrrolopyrrole (DPP)-based polymers, with either a twelve carbon (C12) or a tri ethyleneglycol (TEG) side chains on the DPP units (respectively denoted PCPDTDPP_C12 and PCPDTDPP_TEG). We deposited Langmuir-Schaefer films of these polymers blended with the widely used electron donor material [6,6]-phenyl-C61-butyric-acid methyl ester (PCBM). We then characterized the conformational, optical and morphological properties of these films. From the monolayers to the solid films, we observed distinct self-organization and surface properties for each polymer due to the distinct nature of their side chains. Emphasizing their attraction interactions with PCBM and the phase transitions according to the surface pressure. The elements amount on the surface, calculated through the XPS, gave us a good insight on the polymers' conformations. Through UV-visible absorption spectroscopy, the improvement in the PCPDTDPP film ordering upon PCBM addition is evident and we saw the contribution of the polymer units on the optical response. Chemical attributions of the polymers were assigned using FTIR Spectroscopy and Raman Scattering, revealing the physical interaction after mixing the materials. We showed that it is possible to build nanostructured PCPDTDPPs films with a high control of their molecular properties through an understanding of their self-assembly and interactions with an n-type material.

1. INTRODUCTION

The bulk heterojunction (BHJ) is based on an interpenetrating network of donor (D) and acceptor (A) materials and has given rise to the current, most efficient solar cells, be it in single or in tandem devices [1,2]. Absorption of a photon by the photoactive layer of an organic photovoltaic device (OPV) produces a neutral excited state (exciton) instead of the free charge carriers seen in inorganic photovoltaics. The exciton diffuses to the D/A interface in order to dissociate and form free charge carriers, that can migrate to the respective electrodes. The bicontinuous and interpenetrating network ensures that any light-absorbing site in the bulk-heterojunction (BHJ) is within few nanometers from the D/A interface, while simultaneously allowing the presence of percolation paths towards the electrodes. Respectively, this enhances the quantum efficiency of charge separation, and increases charge collection. The resulting morphology of the phase separated BHJ layer is crucial for the performance of the solar cell [3], and its understanding and control is fundamental to improve device efficiency. Alterations in photovoltaic performance can be obtained by varying the volume ratio of the donor and acceptor phases [4], using different additives [5], processing temperatures [6], and processing solvents [7]. Then, the development of a way to evaluate the materials' interaction and miscibility is critical. Thus, a setup of techniques to characterize the interaction between the active layer materials can be used to perform a previous in-depth analysis that furnish a way to assist the construction of future devices.

The morphology of devices manufactured from organic materials affects significantly their optoelectronic characteristics [8]. In thin films form, the morphology changes can also occur according to the chosen deposition technique. There are many techniques available for the production of films from organic materials [9,10], among them we highlight the Langmuir deposition techniques [11], which provides a mean to evaluate the film even before its transfer to

1
2
3 a solid substrate. Moreover, Langmuir methods are commonly used for the manufacture of films
4
5 in which greater ordering and good control at the molecular level are desired [12]. The Langmuir-
6
7 Blodgett technique is, however, a rather complicated method for making films from non-
8
9 amphiphilic and/or rigid materials [13,14]. For such cases, the Langmuir-Schaefer (LS) technique
10
11 is often preferred, as it removes many of the constraints associated with Langmuir-Blodgett
12
13 techniques [15]. Recently, Noh *et. al* [16] reported the deposition onto different substrates of a
14
15 polymer initially spread onto water to apply as solar cells, therefore, Langmuir analysis may also
16
17 serve as a guide on how is the assembling and possible interactions for who uses such method.
18
19

20
21
22 Among the various polymeric semiconductors that have been studied in recent decades, low-
23
24 bandgap polymers (LBGs) appear as one of the more intriguing donor materials for polymeric
25
26 solar cells [7,17]. This class of π -conjugated polymers shows a better overlap between the
27
28 absorption spectrum of the polymer and the solar spectrum [18–20]. Their absorption towards the
29
30 near infrared (NIR) allows the generation of additional photocurrent, increasing the overall short-
31
32 circuit current, and consequently the efficiency of the cell. In addition, LBGs have more
33
34 delocalized π -electrons, greater conjugation lengths and higher polymer chain planarity when
35
36 compared to other polymers [21,22]. These characteristics lead to a decrease in the energy level of
37
38 the higher occupied molecular orbital (HOMO) of the donor polymer, ease of intermolecular hole
39
40 transport, and a closer (although still often imbalanced) equilibrium in the transport of the electrons
41
42 and holes between the electron donor polymer and the electron acceptor material.
43
44
45

46
47 In this work, we synthesized and characterized the physico-chemical, optical and
48
49 morphological properties of two new LBGs based on the diketopyrrolo[3,4-*c*] pyrrole-1,4-dione
50
51 (DPP) derivative and a cyclopentadithiophene derivative (CPDT), bearing an alkyl and ester side
52
53 chain either by themselves or in a blend with the electron acceptor [6,6]-phenyl-C₆₁-butyric-acid
54
55
56
57
58
59
60

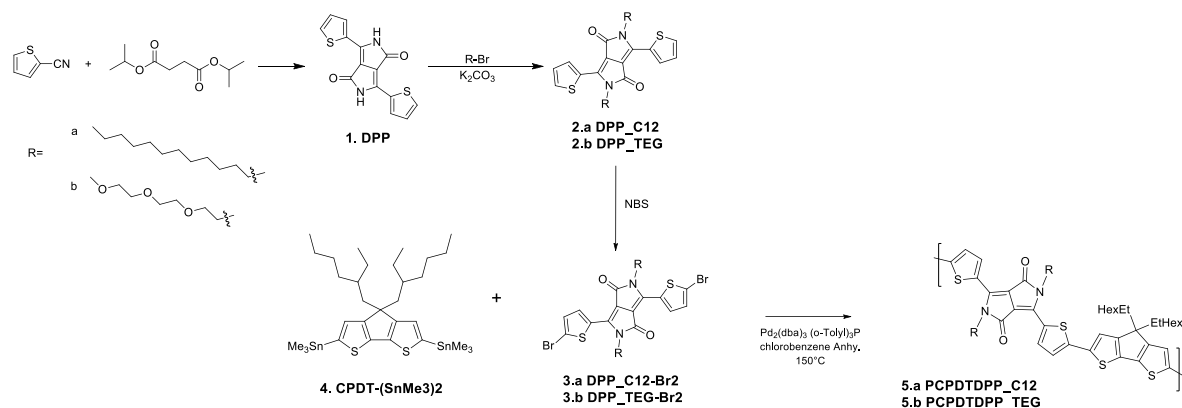
methyl ester (PCBM). BHJ films were fabricated via LS methods. We evaluated the conformation and morphologies of such films aiming to understand the interaction and phase segregation of self-conformation of the low-bandgap polymers and the PCBM.

2. EXPERIMENTAL SECTION

2.1 Materials

Di-isopropylsuccinate, anhydrous iron (III) chloride and anhydrous potassium carbonate (K_2CO_3) were purchased from ABCR. 4,4-Bis(2-ethylhexyl)-2,6-bis(trimethylstannyl)-4H-cyclopenta[2,1-b:3,4-b']dithiophene was purchased from 1-Materials. PCBM and all other reagents and solvents were purchased from Sigma Aldrich. All the chemicals and solvents were used without further purification, unless otherwise stated. All reactions using dry solvents were carried out with oven-dried glassware and under inert atmosphere (N_2), unless otherwise stated.

2.2 Polymers syntheses and characterizations



Scheme 1. Synthesis of PCPDTDPP_C12 and PCPDTDPP_TEG.

The diketopyrrolopyrrole (**DPP**) monomers **3.a** and **3.b** were synthesized according to the synthetic route reported in Scheme 1, adapted from the literature [23]. **DPP** (Scheme 1, **1**) was prepared by reacting 2 equivalents of 2-thiophene-carbonitrile with 1 of di-isopropylsuccinate in

1
2
3 *t*-amyl alcohol. To improve the solubility of the **DPP (1)**, the lactame units should be N-
4 functionalized, preventing the formation of hydrogen bonding between different DPP units. In this
5 work, the DPPs were *N*-alkylated (Scheme 1, **2.a** and **2.b**) using the corresponding bromo-
6 alkanes/ether in presence of K₂CO₃ and 18-crown-6 [23]. Finally, we introduced a suitable
7 polymerizable group on the thiophene units, functionalizing them with bromine atoms by free-
8 radical substitution, using *N*-bromosuccinimide (NBS) as brominating agent (**3.a** and **3.b**).
9

10
11 Poly[4,4'-diethylhexyl-4*H*-cyclopenta[2,1-*b*:3,4-*b'*]dithiophene-*alt*-2,5-didodecyl-3,6-bis
12 (thiophen-2-yl)pyrrolo[3,4-*c*]-pyrrole-1,4-dione], **PCPDTDPP_C12 (5.a)**, and poly[4,4'-
13 diethylhexyl-4*H*-cyclopenta[2,1-*b*:3,4-*b'*]dithiophene-*alt*-2,5-di(2-(2-(2-methoxyethoxy)ethoxy)
14 ethyl-3,6-bis(thiophen-2-yl)pyrrolo[3,4-*c*]pyrrole-1,4-dione], **PCPDTDPP_TEG (5.b)**, were
15 synthesized by Stille polycondensations (Scheme 1), reacting the dibrominated dithieno-**DPPs**
16 monomers (Scheme 1, **3.a** and **3.b**) with 4,4-bis(2-ethylhexyl)-2,6-bis(trimethylstannyl)-4*H*-
17 cyclopenta[2,1-*b*:3,4-*b'*]dithiophene (**CPDT-(SnMe₃)₂**) (Scheme 1, **4**). The polymerizations were
18 performed in anhydrous chlorobenzene with Pd(0) as catalyst at 150 °C for several hours. The
19 Pd(0) was generated *in-situ* from bis(dibenzylideneacetone)-palladium(0) [Pd₂(dba)₃] and tris(2-
20 methylphenyl)phosphine [(*o*-Tolyl)₃P] as ligand [24]. The number average molecular weight, M_n,
21 of the polymers are 15300 g mol⁻¹ and 16200 g mol⁻¹ for the PCPDTDPP_C12 and
22 PCPDTDPP_TEG, respectively.
23
24
25
26
27
28
29
30
31
32
33
34
35
36
37
38
39
40
41
42
43

44 The detailed experimental procedures and chemical characterization are reported in the
45 supporting information (SI).
46
47
48
49

50 **2.3 Instrumentation**

51
52 **2.3.1 Monomer and polymer characterizations.** ¹H-NMR, spectra were recorded on a Bruker
53 (400 MHz) spectrometer; chemical shifts are given relative to tetramethylsilane (TMS). Gel
54
55
56
57
58
59
60

1
2
3 permeation chromatography (GPC) was performed using a bank of 4 columns (Shodex KF801,
4 802.5, 804, and 806), each 300 mm x 8mm at 30 °C with tetrahydrofuran eluent at a flow rate of
5 1.0 mL min⁻¹ controlled by a Malvern pump (Viskotek, VE1122) and connected to Malvern
6 VE3580 refractive index and Malvern VE3210 UV–visible detectors. Conventional calibration
7 was performed against polystyrene standards.
8
9

10
11
12 **2.3.2 Langmuir and LS experiments.** For the fabrication and analysis of the Langmuir films, the
13 low-bandgap polymers and PCBM were dissolved in chloroform at room temperature (23 °C). The
14 Langmuir and LS films were deposited using the Langmuir trough KSV 5000, and its subphase
15 was filled with ultrapure water (Millipore system, resistivity of 18.2 MΩ). The polymer solutions
16 had a concentration of 0.2 mg ml⁻¹, while the PCBM and polymer:PCBM blend (1:1 w/w) of 0.3
17 mg ml⁻¹. Surface pressure isotherms were performed under symmetric barrier compression at a
18 speed of 10 mm min⁻¹, to achieve a target deposition pressure of 20 mN m⁻¹ and 25 mN m⁻¹ for,
19 respectively, monolayers containing PCPDTDPP_C12 and PCPDTDPP_TEG. To fabricate the LS
20 films, we performed consecutive horizontal manual depositions onto solid substrates.
21
22
23
24
25
26
27
28
29
30
31
32
33
34
35
36

37 **2.3.4 Atomic Force Microscopy (AFM).** AFM images of 10 layers LS films deposited onto
38 glass/ITO substrates were recorded in tapping mode using a Park XE7 microscope. The
39 topographic images were analyzed with the proprietary XEI software.
40
41
42
43
44

45 **2.3.5 X-ray Photoelectron Spectroscopy (XPS).** XPS measurements of 10 layers LS films onto
46 ITO substrate were carried out using a K-Alpha X-ray Photoelectron Spectrometer, with a micro-
47 focused monochromatic Al Kα source (Al Kα 1486.6 eV, spot diameter of about 400 μm, power
48 72 W), at a pressure of 2·10⁻⁷ Pa. This equipment utilizes a hemispheric analyzer, a transfer column
49 and a microchannel plate (MCP) detection.
50
51
52
53
54
55
56
57
58
59
60

1
2
3 **2.3.6 UV-visible Absorbance.** The characterization of the optical properties of LBGs and their
4 mixtures with PCBM, both in solution and in thin film on glass substrates, was performed with a
5
6 Varian Cary 100 UV-Visible spectrophotometer.
7
8

9
10 **2.3.7 Raman and Fourier-transform infrared (FTIR) absorption spectroscopy.** The Raman
11 spectra were acquired using a micro-Raman Renishaw spectrograph, model in-Via, coupled to an
12
13 optical Leica microscope (50X objective lens), equipped with a CCD detector and laser at 633 nm.
14
15 The measurements were carried out on films deposited on the golden area of gold interdigitated
16
17 electrode (IDE) on glass substrates (Brazilian Nanotechnology National Laboratory, LNNano) in
18
19 the range between 4000 and 320 cm^{-1} . The FTIR spectra were acquired in the equipment Tensor
20
21 27 from Bruker, in the range from 4000 to 400 cm^{-1} , for the LS films deposited on germanium
22
23 substrates.
24
25
26
27
28
29

30 **3. RESULTS AND DISCUSSIONS**

31
32 **3.1 Langmuir films.** Figure 1 shows the PCBM isotherm. We highlight the presence of a high
33
34 compressibility linear region and the absence of the sharp phase transitions, characteristic of
35
36 amphiphilic molecules. These characteristics give a strong indication that this is a liquid-
37
38 condensed (LC) isotherm, according to Harkins' classification [25]. The calculated area per
39
40 repeating unit for PCBM at the air-water interface was 29 \AA^2 , in good agreement with the literature
41
42 [26]. Moreover, studies on fullerene behaviors spreading onto the air-water interface revealed that
43
44 its films do not form a true monolayer [27,28]. This is due to the non-amphiphilic nature of these
45
46 molecules, together with the aggregation phenomena that arise from strong fullerene-fullerene
47
48 interactions [27,29].
49
50
51
52
53
54
55
56
57
58
59
60

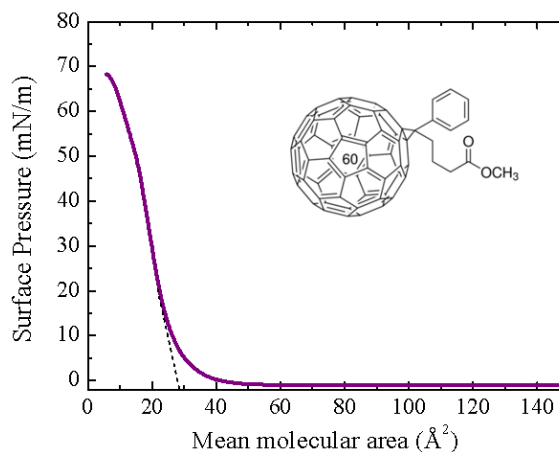


Figure 1. Surface pressure–area isotherms of the PCBM.

In Figure 2, we see the isotherms of the pristine polymers and of their mixture with PCBM attained in the Langmuir trough. The areas per monomer found for these polymers were 68 \AA^2 for PCPDTDPP_C12 (a) and 110 \AA^2 for PCPDTDPP_TEG (b). These values are really low, since the minimum expected surface areas are 242 and 264 \AA^2 for PCPDTDPP_C12 and PCPDTDPP_TEG, respectively, indicating highly coiled polymers within the trough.

The overall polymer isotherms are quite divergent from each other, showing a strong dependence on the side-chains. On the one hand PCPDTDPP_C12 behaves as a liquid-expanded (LE) type, characterized by the absence of a clear phase transition and a reduced compressible linear region. Moreover, this polymer has a rather steady upward trend, until it reaches its collapse pressure at 65 mN m^{-1} . On the other hand, the pressure values of PCPDTDPP_TEG start to raise (corresponding to the transition from the “gas” to the “liquid” state) at a high mean area of 120 \AA^2 . Another steep variation in the slope of the graph occurs at approximately 35 mN m^{-1} , which is associated with the coexistence of two phases [30], and/or the formation of bilayers within the air-water interface in amphiphilic polymers [31]. PCPDTDPP_TEG shows a lower collapse surface pressure (53 mN m^{-1}) than PCPDTDPP_C12 (65 mN m^{-1}), indicating a lower resistance of the monolayer structure to compression [32,33].

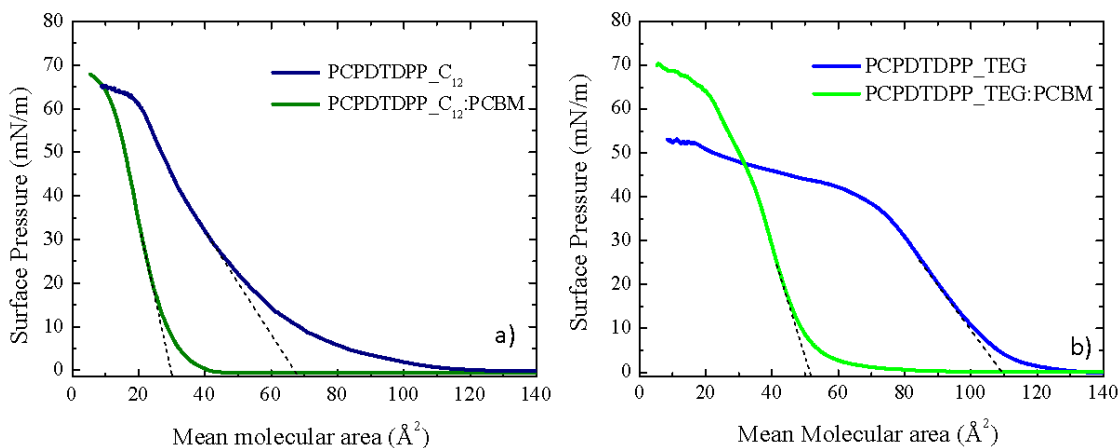


Figure 2. Surface pressure–area isotherms of the a) PCPDTDPP_C12 and b) PCPDTDPP_TEG (in blue), and their mixtures with PCBM (in green)

The PCPDTDPP_C12:PCBM film occupies an area per molecule of 30 \AA^2 , quite close to the area achieved by PCBM itself and the shapes of the respective isotherms are fairly similar (Figure 1). This result indicates that the polymer is not incorporated into the PCBM domains in higher surface pressures, being expelled either to the air phase or to the aqueous subphase. The surface pressure isotherm of PCPDTDPP_TEG:PCBM is closer to that of PCBM than the polymer isotherm, including the collapse pressure value and the LC phase features. Its area per repeating unit (52 \AA^2) is between those of the two separate materials. Therefore, the PCBM molecules seem to be mingled with the polymers' chains of the PCPDTDPP_TEG. However, some parts of the polymer may be lying above the mixed monolayer. This last affirmation is based on the fact that the mean molecular area is below the average between the area of the two materials.

To gain further insight on the phase changes of the monolayers, we calculated the compressibility modulus as $C_s^{-1} = -A \left(\frac{\partial \pi}{\partial A} \right)_T$, where A is the area per molecule/polymer unit, π is the surface pressure and T is the temperature. These graphs are displayed in Figures S.1, where the peaks coincide to the maximum compressibility condition that the monolayers can attain [34].

1
2
3 Through the C_s^{-1} it is possible to ascertain the surface pressure and specific regions of transition,
4
5 by associating C_s^{-1} and tabulated values [35]. In all plots, when the compression starts, C_s^{-1}
6
7 oscillates consistently over zero, due to the lack of, or rather low interaction between the molecules
8
9 over the subphase, corresponding to the “gaseous” phase. At higher compression, an increase in
10
11 the compressibility modulus is observed, pointing that a transition from a gas-like to a more packed
12
13 phase occurs in the films [36]. The maxima of compressibility moduli of all the monolayers but
14
15 the pristine PCPDTDPP_C12, reflected the behavior of a liquid-condensed phase interval
16
17 attribution (100 to 250 mN m⁻¹) [37]. Their maxima were 100, 120, 100 and 150 mN m⁻¹ for the
18
19 PCBM, PCPDTDPP_TEG, PCPDTDPP_C12:PCBM and PCPDTDPP_TEG:PCBM,
20
21 respectively. The peak of C_s^{-1} found for the PCPDTDPP_C12 film (Figure S.1b) was around 70
22
23 mN m⁻¹ corresponding to a liquid-expanded regime. Additionally, the asymmetry of the peaks
24
25 indicates that the phase transition consists of at least two steps, implying that two types of
26
27 reorientation are taking place [38]. These can be either related to the LE-LC transitions within the
28
29 monolayers, or to the rearrangement due to the molecules interactions until reaching the final
30
31 conformation.
32
33
34
35
36

37
38 Comparing the isotherms of the pristine polymers (Figure 2, blue lines) to the isotherms of
39
40 the polymer:PCBM blends (Figure 2, green lines), we also noticed a low miscibility between the
41
42 two materials. Typically, when two materials are miscible with each other the collapse pressure
43
44 value is included between the ones found for the single materials [25]. For both our
45
46 polymer:PCBM mixtures, the collapse pressures are roughly the same as PCBM, indicating the
47
48 PCBM dominant characteristic on the interface. Furthermore, the phase separation and miscibility
49
50 information of mixed monolayers at the air-liquid interface can be obtained quantitatively [39].
51
52 We have analyzed the interactions between the PCPDTDPPs and PCBM within the monolayer in
53
54
55
56
57
58
59
60

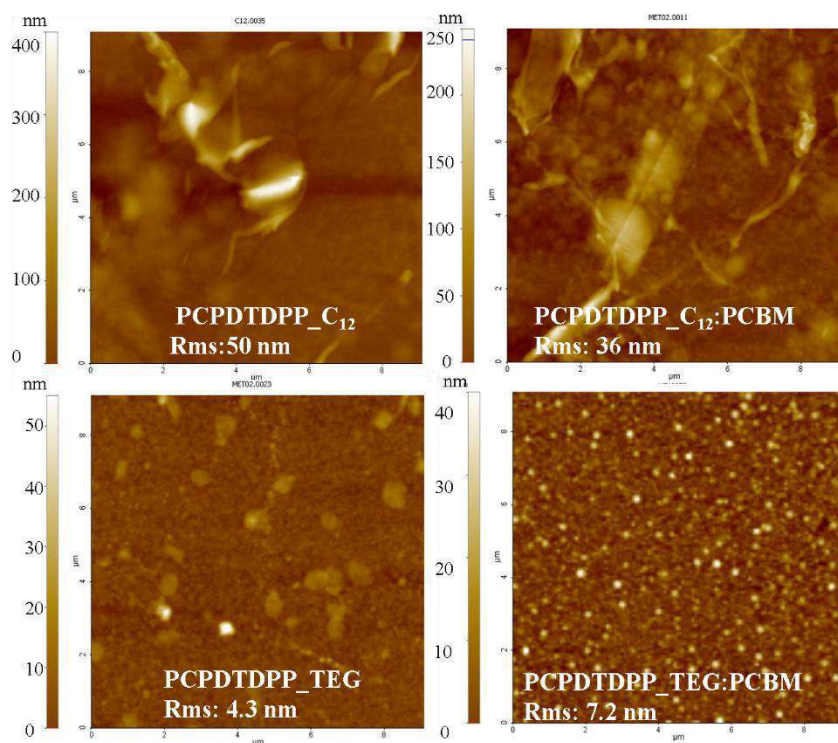
terms of the excess Gibbs free energy of mixing (ΔG_{mix}^{exc}), which can be calculated using the following equation [34]:

$$\Delta G_{mix}^{exc} = \int_0^\Pi (A_{12} - X_1 A_1 + X_2 A_2) d\Pi$$

Where A_{12} is the area per molecule in a two-constituent film, X_i and A_i are the molar fractions and the molecular areas of the constituent i , respectively, at the same pressure. When ΔG_{mix}^{exc} is zero, the interaction between the two components is identical, which means that they are either ideally mixed or not mixed at all [40]. We performed the calculation of the Gibbs excess energy on the surface pressure of the films deposition (20 mN m⁻¹ for the PCPDTDPP_C12 and 25 mN m⁻¹ for the PCPDTDPP_TEG), mainly to observe the compounds behavior on the working settings. The results attained were non-zero revealing that there is a level of miscibility and non-ideal standard behavior of the constituents while they are being compressed. More specifically, the excess areas ($A_E = A_{12} - X_1 A_1 + X_2 A_2$) were negative, -13 Å² for C₁₂ and -11 Å² for the TEG-based polymer, indicating an attractive interaction between the polymers and the PCBM [41]. This information confirms the small areas per unit of the molecules on the trough.

3.2 Atomic Force Microscopy. The 9 x 9 μm² topographic images of the pristine polymer LS films are presented in Figure 3, where the difference in topography between the two films is evident. The PCPDTDPP_C12 film exhibits a quite irregular structure, with big and tall agglomerates and some valleys, while the PCPDTDPP_TEG LS film is more homogeneous. Their root mean square (RMS) roughness are, respectively, 50 nm and 4.3 nm. This finding confirms the isotherms results, because the film with the smaller mean molecular area (PCPDTDPP_C12) at the Langmuir trough presents big polymer agglomerates on the film. For the PCPDTDPP_TEG, which showed a larger surface area over the water and a more homogeneous structure, presumably

1
2
3 by its more hydrophilic properties and inhibition of high aggregation [42] when compared to the
4 alkyl chain of PCPDTDPP_C12, the agglomerates are noticeably smaller. This behavior reflects
5 the different interaction between glycol and alkyl side chains [43,44], which determines the
6
7
8
9
10
11
12
13
14
15
16
17
18
19
20
21
22
23
24
25
26
27
28
29
30
31
32
33
34
35
36
37



38 **Figure 3.** AFM $9 \times 9 \mu\text{m}^2$ images of low-bandgap polymer LS films and their mixtures with PCBM deposited via
39
40
41
42
43
44
45
46
47
48
49
50
51
52
53
54
55
56
57
58
59
60
Langmuir-Schaefer.

43 In Figure 3, we also report the AFM images of polymer:PCBM blends.
44 PCPDTDPP_C12:PCBM shows a higher RMS of 36 nm, compared to the rather flat
45 PCPDTDPP_TEG:PCBM (7.2 nm). After choosing a rather flat area of the
46
47
48
49
50
51
52
53
54
55
56
57
58
59
60

and PCBM, indicated by the more significant topographic inhomogeneities. This validates our hypothesis about the conformation at the air-water interface, where PCPDTDPP_C12 is over the PCBM, while the PCPDTDPP_TEG mixes better with the PCBM forming a single, yet not homogeneous, layer.

3.3 X-ray Photoelectron Spectroscopy (XPS). After AFM and isotherms measurements, the materials proportion in the mixtures still remains an issue. In order to evaluate the amount of PCBM in the polymer:PCBM films, we performed XPS analyses. XPS survey spectra (not shown here) revealed that carbon, oxygen, sulfur and nitrogen elements are present in all the samples. Figure 4 presents C 1s and O 1s high-resolution XPS spectra for PCPDTDPP_C12, PCPDTDPP_TEG and PCPDTDPP_C12:PCBM, PCPDTDPP_TEG:PCBM mixed films.

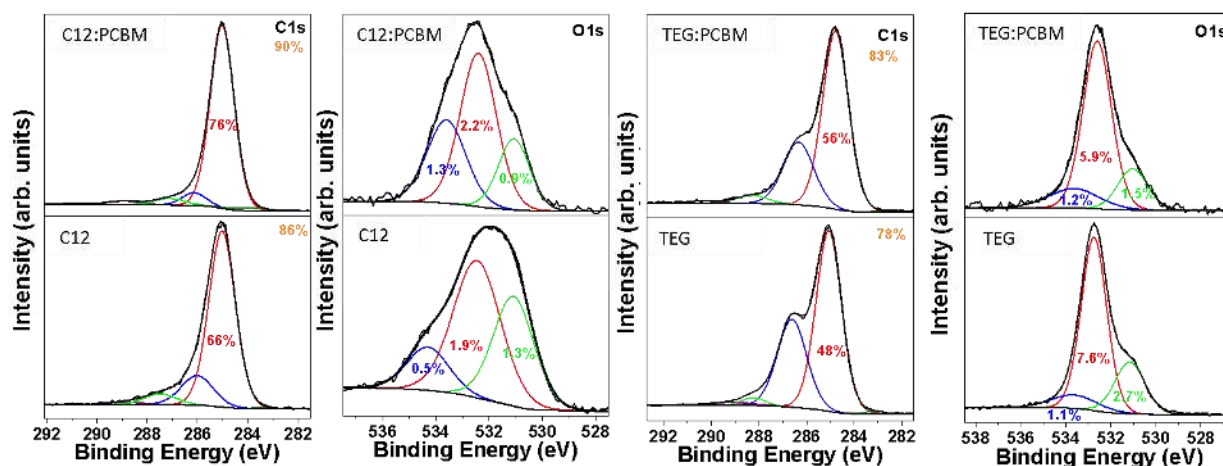


Figure 4. C 1s and O 1s XPS spectra of LS films: PCPDTDPP_C12 and PCPDTDPP_TEG polymers and their mixtures with PCBM.

For PCPDTDPP_TEG, a characteristic C 1s peak is observed at 286.5 eV, which corresponds to $\text{-CH}_2\text{-O}$ and $\text{CH}_3\text{-O}$ environments of carbon (blue component), and a characteristic O 1s peak is observed at 532.7 eV, corresponding to $\text{-CH}_2\text{-O-CH}_2\text{-}$ and $\text{-CH}_2\text{-O-CH}_3$ environments of oxygen

(red component). For both polymers (TEG and C₁₂), a characteristic O 1s peak is observed at 531.1 eV, which corresponds to HN-C=O environment of oxygen (green component). Other C 1s and O 1s peaks cannot be considered as characteristic of these polymers since they are found in PCBM or in the surface contamination of the samples. Therefrom, after PCBM addition to the two polymers we can observe a decrease of their characteristic peaks. At the same time, we observe the increase of the main C 1s peak around 285 eV arising from PCBM addition.

Now, with the objective to quantify in the most accurate way the amount of PCBM at the surface of these samples, we carefully investigated the XPS spectra of the two elements that are absent from PCBM, *i.e.* nitrogen and sulfur. Figure 5 shows N 1s and S 2p high-resolution spectra of these samples. As expected, PCBM addition to the polymers causes a drop of the amount of these two elements.

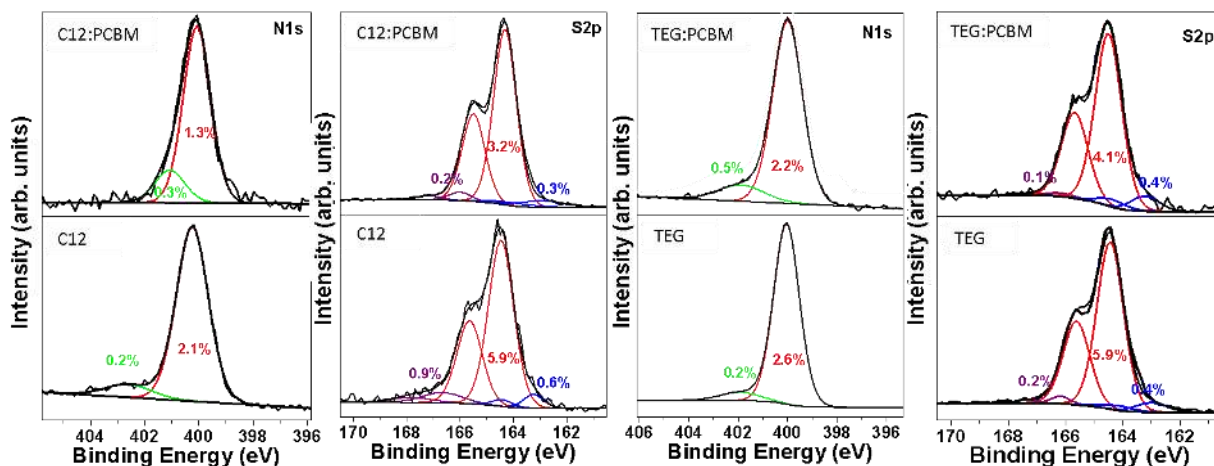


Figure 5. N 1s and S 2p XPS spectra of LS films: PCPDTDPP_C12 and PCPDTDPP_TEG polymers and their mixtures with PCBM.

As nitrogen and sulfur are present only in the polymer and not in PCBM, the proportion of PCBM on the samples surface was determined from the experimental ratios between the total amount of carbon, and the total amounts of sulfur and nitrogen measured by XPS: $X = C_{\text{total}} / (S_{\text{total}} + N_{\text{total}})$. More details about the calculation can be found in the supporting information.

1
2
3 As a result of this analysis, the weight percentage of PCBM at the PCPDTDPP_C12:PCBM and
4 the PCPDTDPP_TEG:PCBM surface is 45% and 24%, respectively. Therefore, we can assert that
5
6
7 PCPDTDPP_C12 mixes well with PCBM, while for PCPDTDPP_TEG the lack of PCBM at the
8
9 surface suggests a different phase segregation, where this material is mainly within the film bulk
10
11 or in more separated domains. Such different phase segregation is consistent with the hydrophilic
12
13 (TEG) and hydrophobic (C12) character of the side chains [43,44]. Taking into account the probe
14
15 depth (~ five nanometers) of this technique, the conformation assumptions made for the Langmuir
16
17 technique may be correct. Where PCPDTDPP_C12 and PCBM form a bilayer of a few molecules
18
19 magnitude - resulting in a comparable amount at the surface - the PCPDTDPP_TEG:PCBM blend
20
21 forms cluster regions, due to their reduced affinity. The high amount of polymer on the surface
22
23 gives origin to clusters, already observed in the AFM images.
24
25
26
27
28

29 **3.4 UV-Visible spectroscopy.** The absorption spectra of the polymer solutions and LS films are
30 shown in Figure 6. The absorption spectrum of PCPDTDPP_C12 in chloroform solution presents
31
32 two bands with maximum absorption (λ_{\max}) centered at 431 and 782 nm, and the corresponding
33
34 LS film also possesses two bands centered at 440 and 754 nm. The PCPDTDPP_TEG solution
35
36 features two absorption bands as well, with λ_{\max} in 424 and 780 nm, whilst in the LS film these
37
38 bands are centered at 444 and 806 nm.
39
40
41
42

43 The first band originates from the CPDT portion, while the largest band, centered at higher
44
45 energy, from the intramolecular charge transfer (ICT) between the CPDT and the DPP units [45].
46
47 The PCPDTDPP_TEG film exhibits a redshift, caused by the strong interaction between the donor-
48
49 acceptor portions within the monomer, depicting a more ordered structure of the material in solid
50
51 state [46,47]. The PCPDTDPP_C12 peak presents a broadening and a blue-shift in the transition
52
53 from solution to film, which are usually attributed to the formation of H-aggregates [48,49]. This
54
55
56
57
58
59
60

type of aggregates is originated, mainly, from the intrachain Coulomb interactions [50], where monomers of different chains stack over one another in a face-on configuration, perpendicular to the molecular plan [51].

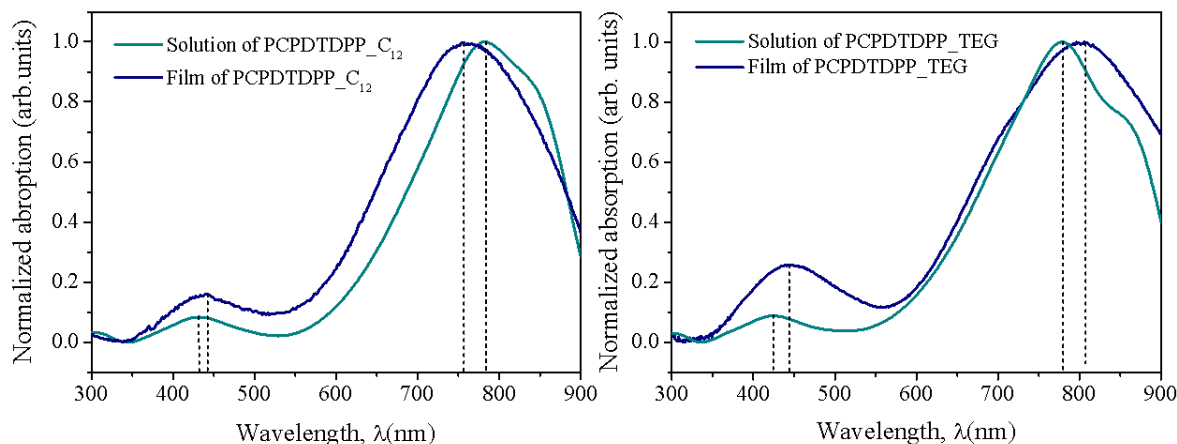


Figure 6. UV-Vis absorption spectra of PCPDTDPP_C12 (a) and PCPDTDPP_TEG samples (b).

Figure 7 shows the absorption spectra of the polymer:PCBM blend in chloroform solution and in the LS films. In the films spectra, the first PCBM peak is shifted from 328 nm to 343 nm. Moreover, an additional absorption band (from 400 to 550 nm) arises, overlapping with a small PCBM peak (430 nm), and the band related to the PCPDTDPP_C12 is at 781 nm. Concerning the aforementioned LS films, there is a shift with respect to that of solution in the spectrum, particularly for the PCBM peak from 328 nm to 335 nm and the polymer band from 779 to 812 nm. In addition, an intermediary band centered at 435 nm emerges, which is related to the CPDT portion.

Thereafter, with regard to the mixed films, comparing the solutions to the solid films, the overall behavior is that the PCBM peak is redshifted for both polymer:PCBM mixtures. On the other hand, the band associated to the interaction between the polymer portions does not change for the PCPDTDPP_C12:PCBM, whilst for the PCPDTDPP_TEG:PCBM it redshifts of 33 nm. Thereby for both mixed films a certain degree of general ordering and a greater conjugation length

are emerging when they pass to film form [52]. Correlating these results to the pristine films, the blends demonstrate an enhancement of the structural organization caused by the molecular rearrangement of the polymers backbone upon the grafting of the PCBM moieties.

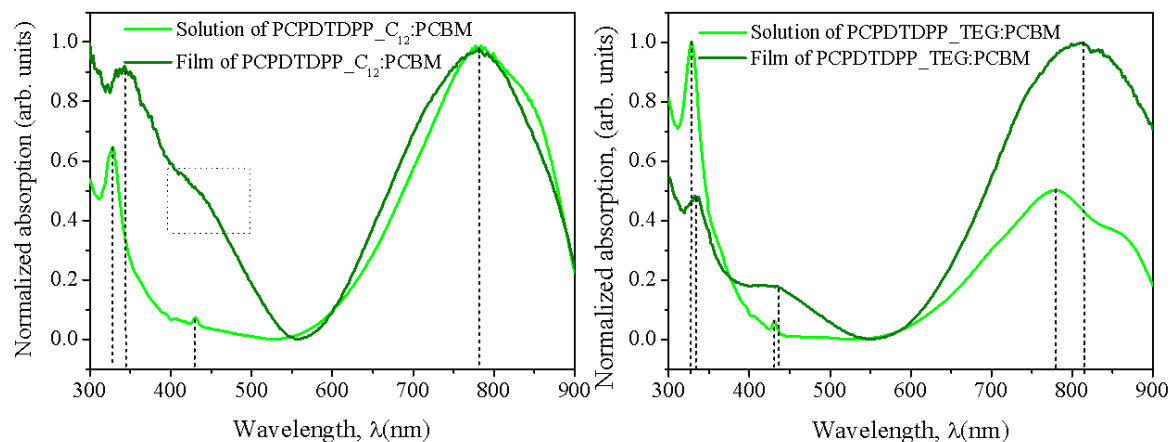


Figure 7. UV-Vis absorption spectra of PCPDTDPP_C12:PCBM (a) and PCPDTDPP_TEG:PCBM (b) samples.

3.5 Raman spectroscopy. The Raman spectra (excitation laser line at 633 nm) of PCBM and low-bandgap polymers as bulky neat materials are presented in Figure 8. The PCBM (Figure 8.a) shows a strong photoluminescence signal [53,54], preventing the observation of any Raman bands. The spectra of the polymers PCPDTDPP_C12 and PCPDTDPP_TEG shown in Figure 8.b) and .c), respectively, are similar, presenting quite the same center positions and relative intensities for the Raman bands. There are three strong bands at 1512, 1409 and 1364 cm^{-1} , which are tentatively attributed to thiophene C=C/C-C stretching/shrinking, thiophene ring C=C stretching, and DPP C=C and (C-N+C-C) stretching modes, respectively, as reported for similar polymers [55–57]. Other well-defined bands are seen at 1229 cm^{-1} and assigned to C-H bending, at 1075 cm^{-1} to C-N and C-H stretching, and at 709 cm^{-1} to C-S stretching modes [56,58]. Moreover, there is a broad band from 2740 to 2900 cm^{-1} , which is related to C-H and C=O stretching modes [59].

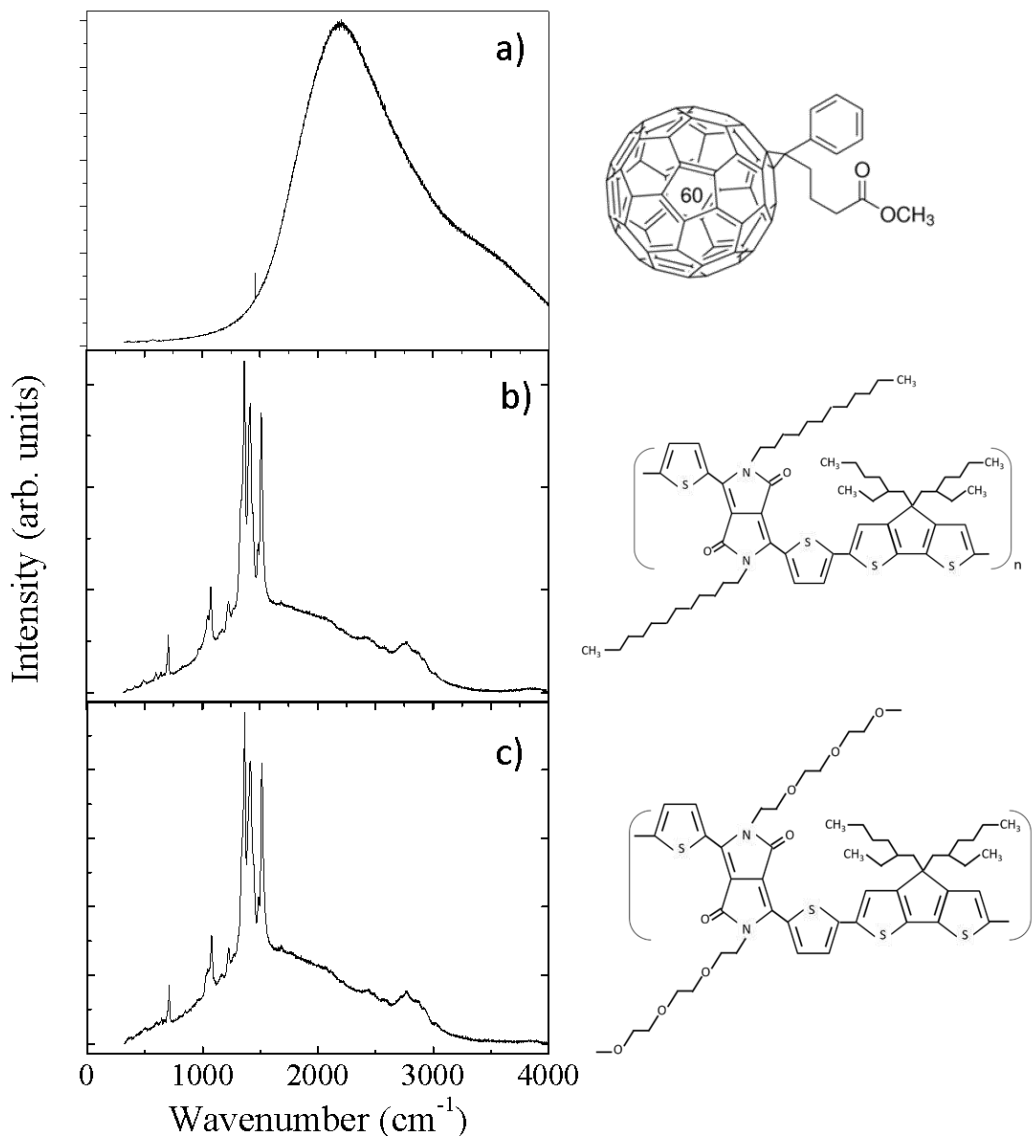


Figure 8. Raman spectra for a) PCBM, b) PCPDTDPP_C12 and c) PCPDTDPP_TEG LS films. Laser line: 633 nm.

We also measured the Raman scattering of the LS films of the polymer:PCBM mixtures. The spectra were taken from different regions of the films in order to analyze the morphology/composition and possible interactions. In Figure 9 displays the optical image of the LS film of PCPDTDPP_C12:PCBM with the Raman spectra of four distinct regions. It is possible to notice the fluorescence band from the PCBM (around 2200 cm^{-1}) and the characteristic Raman bands of the polymers. This confirms the presence of both materials forming the LS films onto

1
2
3 IDE electrodes. Besides, the absence of new bands or significant spectral changes, such as center
4 shift and relative intensities, indicate the materials keep their chemical integrity (no chemical
5 interactions) even several days after fabricating the films. Concerning composition yet, the black
6 spots on the optical image show a stronger relative PCBM fluorescence band (Figure 9.e), which
7 indicates higher concentration of PCBM in this region.
8
9
10
11
12
13
14
15
16
17
18
19
20
21
22
23
24
25
26
27
28
29
30
31
32
33
34
35
36
37
38
39
40
41
42
43
44
45
46
47
48
49
50
51
52
53
54
55
56
57
58
59
60

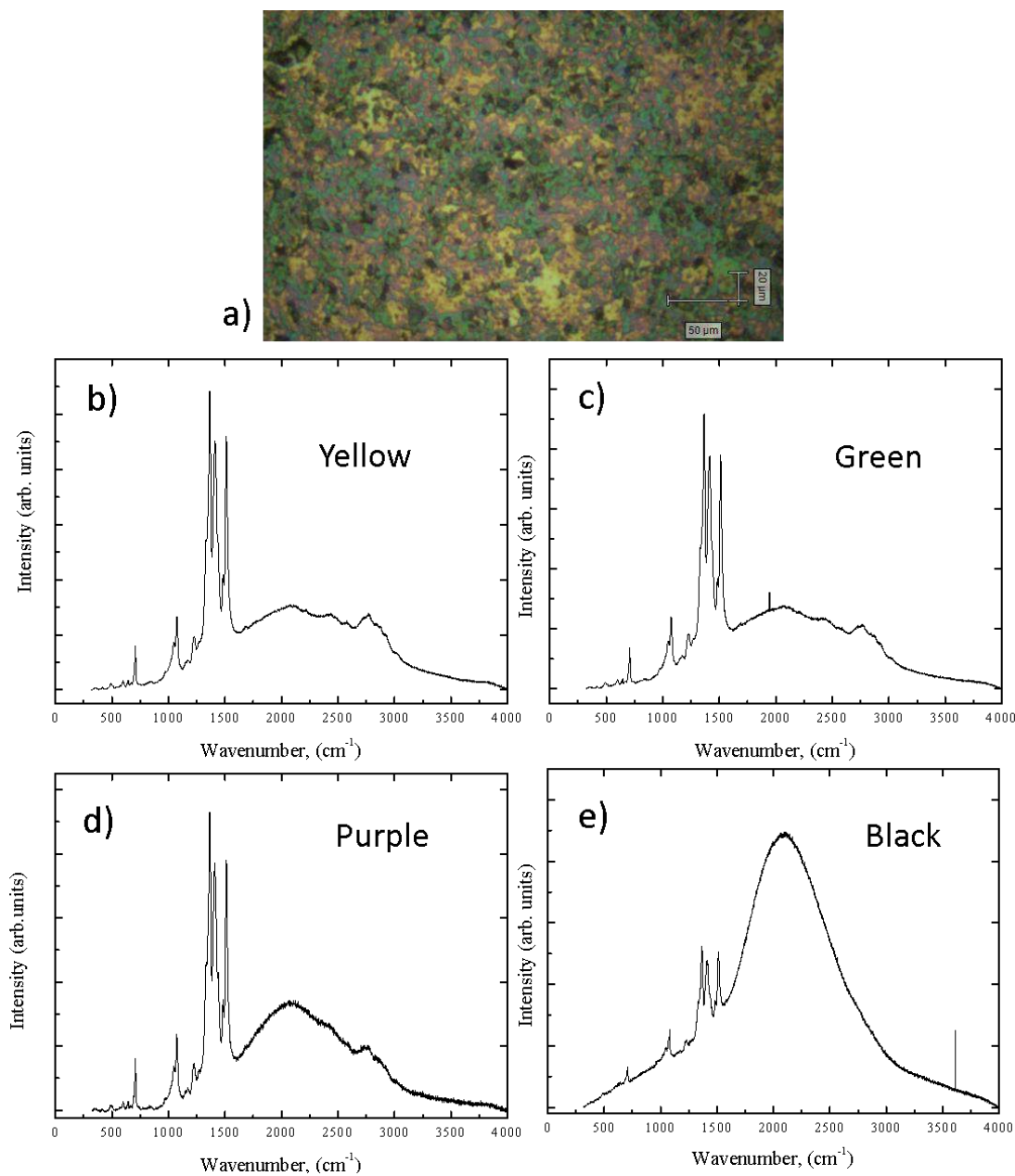


Figure 9. Optical microscopy image (500X magnification) of film LS of PCPDTDPP_C12:PCBM (a) and the Raman spectra for different regions of the films (b, c, d and e). Laser line: 633 nm.

Performing the same measurements for the PCPDTDPP_TEG:PCBM LS films, the Raman spectra are shown in Figure 10. This film presents three different regions: the two light regions (Figure 10.a and b) show the same behavior of the other polymer:PCBM blend, indicating the presence of both materials forming the sample and only physical interaction has occurred.

Notwithstanding, the black clusters reveal only the PCBM fluorescence band on its spectrum, which demonstrates the absence or remarkably low amount of the polymer in such region.

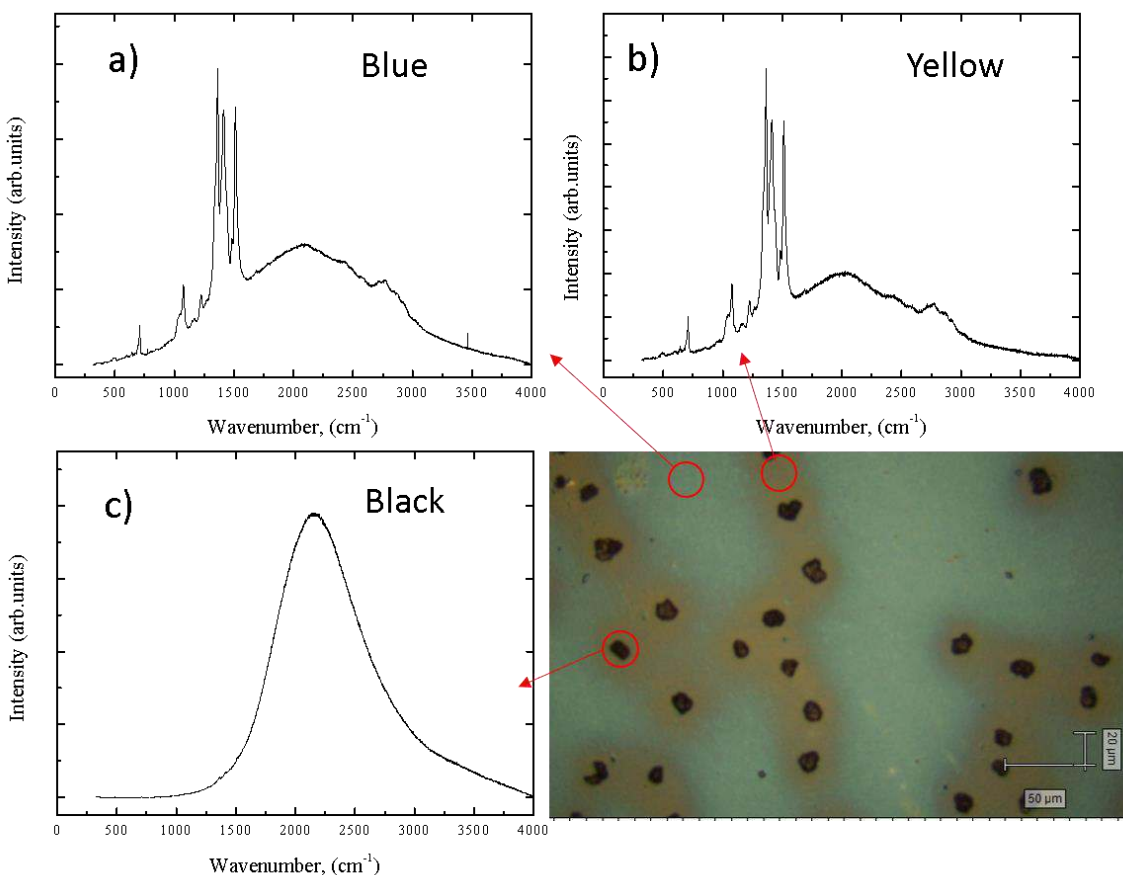


Figure 10. Optical microscopy image (500X magnification) of film LS of PCPDTDPP_TEG:PCBM and the Raman spectra for different regions of the films (x and y).

Thus, the LS film morphology of the two polymers when mixed with PCBM has different features, with PCPDTDPP_C12 showing higher miscibility with PCBM compared to PCPDTDPP_TEG, where PCPDTDPP_C12 PCPDTDPP_TEG well-defined clusters of PCBM are visible. These aggregates are probably already formed in the Langmuir trough during the compression of such films, as suggested by the compression isotherm areas and the attraction interaction from the excess area of Gibbs free energy.

1
2
3 **3.6 FTIR Spectroscopy.** As a complement for the Raman scattering analysis, FTIR absorption
4 spectroscopy measurements were performed. The chemical composition of the pristine polymers
5 and their mixture with PCBM was observed using FTIR results. Figure 11 shows the measured
6 FTIR spectra of the PCBM, PCPDTDPP_C12 and PCPDTDPP_C12:PCBM mixed samples.
7 Figure 11.a reports the PCBM spectrum; the absorption bands at 2918 and 2850 cm^{-1} are attributed
8 to asymmetric and symmetric C-H stretching modes in CH_2 groups, respectively. The peak at 1737
9 cm^{-1} corresponds to C=O group, at 754 cm^{-1} to Aryl-H bending vibration, and other peaks at 526,
10 1186 and 1424 cm^{-1} are the characteristic peaks of fullerene [60–62]. PCPDTDPP_C12 (Figure
11.b) spectrum contains the peaks associated to C-H stretching (2920 and 2850 cm^{-1}), C=O of the
12 DPP unit (1664 cm^{-1}) and C=C and C-C stretching modes of thiophene (1510 to 1545 cm^{-1}). We
13 identified the C-H bending and the C-N stretching modes (1438 to 1460 cm^{-1}), the C=C stretching
14 of the thiophene ring (1404 cm^{-1}), the C=C and (C-N+C-C) stretching modes (1377 cm^{-1}) localized
15 on the DPP unit [33,63,64]. The peaks between 980 and 1300 cm^{-1} correspond to the C-S stretching
16 and C-H bending coupled to thiophene ring stretches, and at 806 cm^{-1} to C-H out of plane [65].
17
18
19
20
21
22
23
24
25
26
27
28
29
30
31
32
33
34

35 As for the PCPDTDPP_C12:PCBM blend ((Figure 11.c), the results are quite similar to the
36 polymer, with a more defined C=O peak due to the presence of PCBM, nevertheless, no chemical
37 interaction seems to be present, consistent with Raman scattering results.
38
39
40
41
42
43
44
45
46
47
48
49
50
51
52
53
54
55
56
57
58
59
60

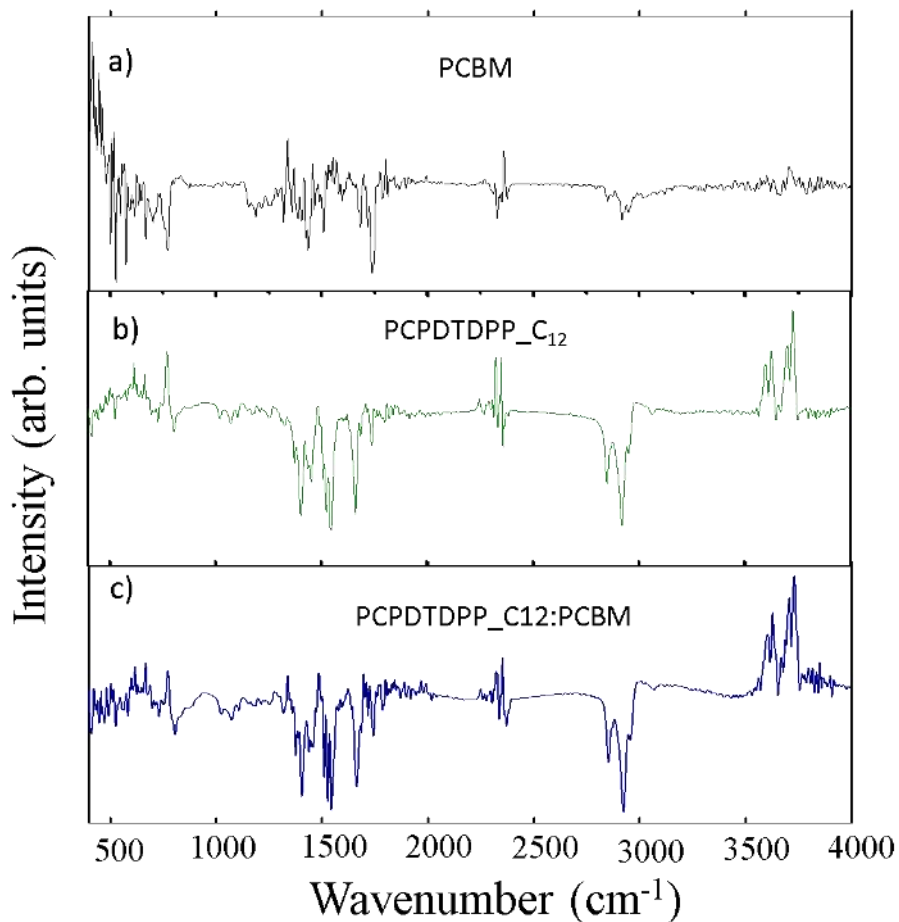


Figure 11. FTIR spectra recorded from drop-cast films of a) PCBM, b) PCPDTDPP_C12 and c) PCPDTDPP_C12:PCBM on Ge (transmission mode).

Figure 12 depicts the FTIR spectra of the PCPDTDPP_TEG:PCBM blend and of the two separate materials. The pristine PCPDTDPP_TEG spectra is similar to that of PCPDTDPP_C12. The most noteworthy difference is the presence of the C-O-C asymmetric stretching mode between 1000-1150 cm⁻¹ (Figure 12.b, circled) due to the different side chain (TEG). For this polymer as well, the interaction between the polymer and the PCBM was merely physical.

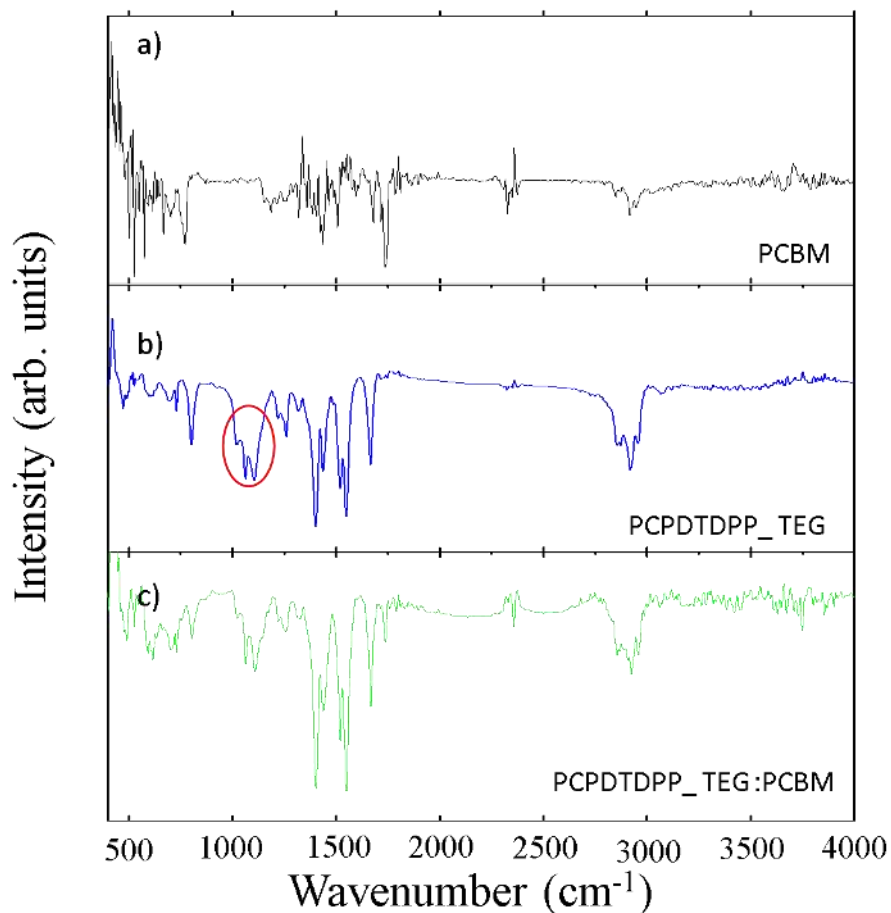


Figure 12. FTIR spectra recorded from drop-cast films of a) PCBM, b) PCPDTDPPE_TEG and c) PCPDTDPPE_TEG:PCBM on Ge (transmission mode).

To investigate the film stability, we recorded over 1 month FTIR spectra of the films exposed to air in the dark. We did not observe any significant variation during this period. The PCBM band centered at 1750 cm⁻¹ appears clearly in the mixture, however apparently did not occur any shifts/inversions or upsurge of bands.

4. CONCLUSIONS

Structural, morphological and conformational investigations of pristine PCPDTDPPE_C12 and PCPDTDPPE_TEG LS films, as well as their BHJ configuration with PCBM were performed. Langmuir films revealed the influence of the DPP unit branch of each polymer on the monolayer

1
2
3 conformation. The insertion of PCBM at the Langmuir trough showed the remarkable interaction
4 of the polymers with this fullerene derivative, although this interaction resulted in different
5 conformation with each polymer. There was no chemical interaction and some miscibility between
6 the polymers and PCBM in a BHJ configuration. The amount of the PCBM on the mixed films
7 surfaces presented substantial discrepancy, confirming the disparity of the polymers self-assemble
8 onto the substrates. Through absorption spectra we noticed that the introduction of PCBM into the
9 polymer thin films improved the structural molecular arrangement. These assessments provided
10 many information concerning this class of polymers in its pristine form or blended with a known
11 electron acceptor in OPVs. Therefore, it opens the way for evaluating intra- and intermolecular
12 interactions responsible for the development of optoelectronic devices.
13
14
15
16
17
18
19
20
21
22
23
24
25
26

27 ASSOCIATED CONTENTS

28 Supplementary information

29 Full description of the monomer and polymer synthesis procedures, ¹H NMR spectra and the
30 Compressibility modulus plots.
31
32
33
34
35

36 ACKNOWLEDGMENTS

37
38 The authors are grateful for the financial support of the Brazilian agencies CAPES, CNPq-SWE
39 [Grant number 205489/2014-1], FAPESP [Grant numbers 2014/13739-7 and 2014/11410-8],
40 INEO/CNPq.
41
42
43
44
45

46 REFERENCES

- 47
48 [1] Wang Y, Ke X, Xiao Z, Ding L, Xia R and Yip H 2018 Organic and solution-processed
49 tandem solar cells with 17.3% efficiency *Science (80-.)*. **1098** 1094–8
50
51 [2] Wadsworth A, Moser M, Marks A, Little M S, Gasparini N and Brabec C J 2019 Critical
52 review of the molecular design progress in non-fullerene electron acceptors towards
53 commercially viable organic solar cells † *Chem. Soc. Rev.* **48** 1596–625
54
55 [3] Heeger A J 2010 Semiconducting polymers: the Third Generation *Chem. Soc. Rev.* **39** 2354
56
57
58
59
60

- 1
2
3 [4] Li C, Li Y, Wang X, Zhang B and Chen Y 2015 Synthesis and photovoltaic properties of
4 conjugated copolymers containing cyclopentadithiophene and two different electron-
5 deficient moieties in the polymer backbone *J. Polym. Res.* **22**
6
7 [5] Holliday S, Li Y and Luscombe C K 2017 Progress in Polymer Science Recent advances
8 in high performance donor-acceptor polymers for organic photovoltaics *Prog. Polym. Sci.*
9 **70** 34–51
10
11 [6] Miller S, Fanchini G, Lin Y-Y, Li C, Chen C-W, Su W-F and Chhowalla M 2008
12 Investigation of nanoscale morphological changes in organic photovoltaics during solvent
13 vapor annealing *J. Mater. Chem.* **18** 306
14
15 [7] Bundgaard E and Krebs F C 2007 Low band gap polymers for organic photovoltaics *Sol.*
16 *Energy Mater. Sol. Cells* **91** 954–85
17
18 [8] de Boer B, van Hutten P F, Ouali L, Grayer V and Hadziioannou G 2002 Amphiphilic,
19 Regioregular Polythiophenes *Macromolecules* **35** 6883–92
20
21 [9] Pavinatto F J, Caseli L and Oliveira O N 2010 Chitosan in nanostructured thin films
22 *Biomacromolecules* **11** 1897–908
23
24 [10] Gaffo L, Zucolotto V, Cordeiro M R, Moreira W C, Oliveira O N, Cerdeira F and Brasil M
25 J S P 2007 Structural aspects of Langmuir–Blodgett and cast films of zinc phthalocyanine
26 and zinc hexadecafluorophthalocyanine *Thin Solid Films* **515** 7307–12
27
28 [11] Rodríguez R, Ignés-Mullol J, Sagués F, Quiñoá E, Riguera R and Freire F 2016 Helical
29 sense selective domains and enantiomeric superhelices generated by Langmuir–Schaefer
30 deposition of an axially racemic chiral helical polymer *Nanoscale* **8** 3362–7
31
32 [12] Braunger M L, Barros A, Ferreira M and Olivati C A 2015 Electrical and electrochemical
33 measurements in nanostructured films of polythiophene derivatives *Electrochim. Acta* **165**
34 1–6
35
36 [13] Aoki Atsushi and Fukuyama Shinya 2010 Organic Thin Film Solar Cell Composed of
37 Hetero-Deposited Langmuir-Blodgett Films *Electrochemistry* **78** 178–80
38
39 [14] Sołoducho J, Cabaj J and Swist A 2009 Structure and sensor properties of thin ordered solid
40 films. *Sensors (Basel)*. **9** 7733–52
41
42 [15] Ram M K, Adami M, Sartore M, Salerno M, Paddeu S and Nicolini C 1999 Comparative
43 studies on Langmuir-Schaefer films of polyanilines *Synth. Met.* **100** 249–59
44
45 [16] Noh J, Jeong S and Lee J-Y 2016 Ultrafast formation of air-processable and high-quality
46 polymer films on an aqueous substrate. *Nat. Commun.* **7** 12374
47
48 [17] Etxebarria I, Ajuria J and Pacios R 2015 Polymer: fullerene solar cells: materials,
49 processing issues, and cell layouts to reach power conversion efficiency over 10%, a
50 review *J. Photonics Energy* **5** 1–25
51
52 [18] Nelson J 2002 Organic photovoltaic films *Curr. Opin. Solid State Mater. Sci.* **6** 87–95
53
54
55
56
57
58
59
60

- 1
2
3 [19] Neugebauer H, Kvarnström C, Brabec C, Sariciftci N S, Kiebooms R, Wudl F and Luzzati
4 S 1999 Infrared spectroelectrochemical investigations on the doping of soluble
5 poly(isothianaphthene methine) (PIM) *J. Chem. Phys.* **110** 12108
6
7 [20] Brabec B C J, Winder C, Sariciftci N S, Hummelen J C, Dhanabalan A, Hal P A Van and
8 Janssen R A J 2002 A Low-Bandgap Semiconducting Polymer for Photovoltaic Devices
9 and Infrared Emitting Diodes *Adv. Funct. Mater.* **12** 709–12
10
11 [21] Li Y 2012 Molecular Design of Photovoltaic Materials for Polymer Solar Cells : Toward
12 Suitable Electronic Energy Levels and Broad Absorption *Acc. Chem. Res.* **45** 723–33
13
14 [22] Chen H, Hou J, Zhang S, Liang Y, Yang G and Yang Y 2009 Polymer solar cells with
15 enhanced open-circuit voltage and efficiency *Nat. Photonics* **3** 649–53
16
17 [23] Li Y 2009 Diketopyrrolopyrrole-based derivatives for thin film transistors (EP2034537
18 (A2)) 44
19
20 [24] V. Farina, V. Krishnamurthy W J S 1997 The Stille Reaction *Org. React.* **50** 3–664
21
22 [25] Gareth Roberts 1990 *Langmuir-Blodgett Films* vol 1, ed G Roberts (Boston, MA: Springer
23 US)
24
25 [26] Petty M C 1996 *Langmuir-Blodgett Films: an introduction* (Cambridge: Cambridge
26 University Press)
27
28 [27] Lindemann W R, Wang W, Fungura F, Shinar J, Shinar R and Vaknin D 2014 The effect
29 of cesium carbonate on 1-(3-methoxycarbonyl)propyl-1-phenyl[6,6]C₆₁ aggregation in
30 films *Appl. Phys. Lett.* **105** 1–5
31
32 [28] Maliszewskyj N C, Heiney P A, Jones D R, Strongin R M, Cichy M A and Smith A B 1993
33 Langmuir Films of C₆₀, C₆₀O, and C₆₁H₂ *Langmuir* **9** 1439–41
34
35 [29] Marczak R, Hoang V T, Noworyta K, Zandler M E, Kutner W and D'Souza F 2002
36 Molecular recognition of adenine, adenosine and ATP at the air–water interface by a uracil
37 appended fullerene *J. Mater. Chem.* **12** 2123–9
38
39 [30] Hwang M J and Kim K 1999 Poly(ethylenimine) as a subphase stabilizer of stearic acid
40 monolayers at the air/water interface: surface pressure-area isotherm and infrared
41 spectroscopy study *Langmuir* **15** 3563–9
42
43 [31] Braunger M L, da Silva E A, Awada H, de Oliveira V J, Silva H S, Bégué D, Hiorns R C,
44 Lartigau-Dagron C and de Almeida Olivati C 2018 Langmuir and Langmuir-Blodgett films
45 of low-bandgap polymers *Polym. Int.* **67** 1028–34
46
47 [32] Pawlicka A, Faria R and Yonashiro M 1994 Effect of polymer molecular weight on
48 Langmuir monolayers and the deposition of Langmuir-Blodgett films of poly (3-
49 butylthiophene) and stearic acid *Thin Solid Films* **244** 723–7
50
51 [33] Silva E A da, Caseli L and Olivati C de A 2017 Organization of polythiophenes at ultrathin
52 films mixed with stearic acid investigated with polarization-modulation infrared reflection–
53
54
55
56
57
58
59
60

- absorption spectroscopy *Colloids Surfaces A Physicochem. Eng. Asp.* **529** 628–33
- [34] Rodrigues de Oliveira V J, Assunção da Silva E, Braunger M L, Awada H, de Santana H, Hiorns R C, Lartigau-Dagron C and de Almeida Olivati C 2018 Molecular organization relationship of low-bandgap polymers at the air-water interface and in solid films *J. Mol. Liq.* **268** 114–21
- [35] Dennison S R, Harris F and Phoenix D A 2010 A Langmuir approach using on monolayer interactions to investigate surface active peptides. *Protein Pept. Lett.* **17** 1363–75
- [36] Belegriou S, Dorn J, Kreiter M, Kita-Tokarczyk K, Sinner E-K and Meier W 2010 Biomimetic supported membranes from amphiphilic block copolymers *Soft Matter* **6** 179
- [37] Davies J T and Rideal E K 2007 *Interfacial Phenomena* ed C Miller and Neogi (CRC Press)
- [38] Yu Z W, Jin J and Cao Y 2002 Characterization of the liquid-expanded to liquid-condensed phase transition of monolayers by means of compressibility *Langmuir* **18** 4530–1
- [39] Gaines G L 1966 Thermodynamic relationships for mixed insoluble monolayers *J. Colloid Interface Sci.* **21** 315–9
- [40] Nakahara H, Hirano C, Fujita I and Shibata O 2013 Interfacial Properties in Langmuir Monolayers and LB Films of DPPC with Partially Fluorinated Alcohol (F8H7OH) *J. Oleo Sci.* **62** 1017–27
- [41] Modlińska A and Bauman D 2011 The Langmuir-Blodgett technique as a tool for homeotropic alignment of fluorinated liquid crystals mixed with arachidic acid *Int. J. Mol. Sci.* **12** 4923–45
- [42] Lei T, Wang J, Pei J, Lei T, Wang J and Pei J 2014 Roles of Flexible Chains in Organic Semiconducting Materials Roles of Flexible Chains in Organic Semiconducting Materials *Chem. Mater.* **26** 594–603
- [43] Chen X, Zhang Z, Ding Z, Liu J and Wang L 2016 Diketopyrrolopyrrole-based Conjugated Polymers Bearing Branched Oligo(Ethylene Glycol) Side Chains for Photovoltaic Devices *Angew. Chemie - Int. Ed.* **55** 10376–80
- [44] Yang S F, Liu Z T, Cai Z X, Dyson M J, Stingelin N, Chen W, Ju H J, Zhang G X and Zhang D Q 2017 Diketopyrrolopyrrole-Based Conjugated Polymer Entailing Triethylene Glycols as Side Chains with High Thin-Film Charge Mobility without Post-Treatments *Adv. Sci.* **4**
- [45] Chen G, Chiang C, Kekuda D, Lan S, Chu C and Wei K 2010 Synthesis and Characterization of a Narrow-Bandgap Polymer Containing Alternating Cyclopentadithiophene and Diketo-Pyrrolo-Pyrrole Units for Solar Cell Applications *J. Polym. Sci. Part A Polym. Chem.* **48** 1669–75
- [46] Punzi A, Nicoletta F, Marzano G, Fortuna C G, Dagar J, Brown T M and Farinola G M 2016 Synthetic Routes to TEG-Substituted Diketopyrrolopyrrole-Based Low Band-Gap Polymers *European J. Org. Chem.* **2016** 3233–42

- 1
2
3 [47] Sun Y, Welch G C, Leong W L, Takacs C J, Bazan G C and Heeger A J 2012 Solution-
4 processed small-molecule solar cells with 6.7% efficiency. *Nat. Mater.* **11** 44–8
5
6 [48] Saini R, Mahajan A, Bedi R K, Aswal D K and Debnath a. K 2014 Solution processed
7 films and nanobelts of substituted zinc phthalocyanine as room temperature ppb level Cl₂
8 sensors *Sensors Actuators, B Chem.* **198** 164–72
9
10 [49] Ehrenreich P, Birk S T, Zimmermann E, Hu H, Kim K, Weickert J, Pfadle T and Schmidt-
11 mende L 2016 H-aggregate analysis of P3HT thin films-Capability and limitation of
12 photoluminescence and UV / Vis spectroscopy **2** 1–8
13
14 [50] Spano F C and Silva C 2014 H- and J-Aggregate Behavior in Polymeric Semiconductors
15 *Rev. Adv.* **65** 477–500
16
17 [51] Pescitelli G, Di Bari L and Berova N 2014 Application of electronic circular dichroism in
18 the study of supramolecular systems. *Chem. Soc. Rev.* **43** 5211–33
19
20 [52] Chittibabu, KG; Li, L; Kamath M 1994 Synthesis and properties of a novel polythiophene
21 derivative with a side-chain NLO chromophore *Chem. Mater.* **6** 475–80
22
23 [53] Wang X, Zhang D, Braun K, Egelhaaf H J, Brabec C J and Meixner A J 2010 High-
24 Resolution spectroscopic mapping of the chemical contrast from nanometer domains in
25 P3HT:PCBM organic blend films for Solar-Cell applications by *Adv. Funct. Mater.* **20** 492–
26 9
27
28 [54] Wang X, Egelhaaf H J, Mack H G, Azimi H, Brabec C J, Meixner A J and Zhang D 2014
29 Morphology related photodegradation of low-band-gap polymer blends *Adv. Energy Mater.*
30 **4** 1–12
31
32 [55] Francis C, Fazzi D, Grimm S B, Paulus F, Beck S, Hillebrandt S, Pucci A and Zaumseil J
33 2017 Raman spectroscopy and microscopy of electrochemically and chemically doped
34 high-mobility semiconducting polymers *J. Mater. Chem. C* **5** 6176–84
35
36 [56] Roy P, Jha A, Yasarapudi V B, Ram T, Puttaraju B, Patil S and Dasgupta J 2017 Ultrafast
37 bridge planarization in donor- π -acceptor copolymers drives intramolecular charge transfer
38 *Nat. Commun.* **8**
39
40 [57] Wood S, Wade J, Shahid M, Collado-Fregoso E, Bradley D D C, Durrant J R, Heeney M
41 and Kim J-S 2015 Natures of optical absorption transitions and excitation energy dependent
42 photostability of diketopyrrolopyrrole (DPP)-based photovoltaic copolymers *Energy*
43 *Environ. Sci.* **8** 3222–32
44
45 [58] Calvo-Castro J, Warzecha M, McLean A J and McHugh C J 2016 Impact of substituent
46 effects on the Raman spectra of structurally related N-substituted diketopyrrolopyrroles *Vib.*
47 *Spectrosc.* **83** 8–16
48
49 [59] Doris M, Aziz F, Alhummiyany H, Bawazeer T, Alsenany N, Mahmoud A, Zakaria R,
50 Sulaiman K and Supangat A 2017 Determining the Effect of Centrifugal Force on the
51 Desired Growth and Properties of PCPDTBT as p-Type Nanowires *Nanoscale Res. Lett.* **12**
52 1–11
53
54
55
56
57
58
59
60

- 1
2
3 [60] Sharma T, Singhal R, Vishnoi R, Sharma P, Patra A, Chand S, Lakshmi G B V S and
4 Biswas S K 2016 Electronic excitation induced modifications of optical and morphological
5 properties of PCBM thin films *Nucl. Instruments Methods Phys. Res. Sect. B Beam Interact.*
6 *with Mater. Atoms* **379** 176–80
7
8 [61] Wu J, Yue G, Xiao Y, Ye H, Lin J and Huang M 2010 Application of a polymer
9 heterojunction in dye-sensitized solar cells *Electrochim. Acta* **55** 5798–802
10
11 [62] Yoo S H, Kum J M and Cho S O 2011 Tuning the electronic band structure of pcbm by
12 electron irradiation *Nanoscale Res. Lett.* **6** 1–7
13
14 [63] Jiang X, Ding J and Kumar A 2008 Polyurethane-poly(vinylidene fluoride) (PU-PVDF)
15 thin film composite membranes for gas separation *J. Memb. Sci.* **323** 371–8
16
17 [64] Weber C D, Bradley C and Lonergan M C 2014 Solution phase n-doping of C₆₀ and PCBM
18 using tetrabutylammonium fluoride *J. Mater. Chem. A* **2** 303–7
19
20 [65] Kelkar D and Chourasia A 2013 Electrical and Magnetic Conduction Properties of
21 Polythiophene Doped with FeCl₃ *Macromol. Symp.* **327** 45–53
22
23
24
25
26
27
28
29
30
31
32
33
34
35
36
37
38
39
40
41
42
43
44
45
46
47
48
49
50
51
52
53
54
55
56
57
58
59
60